

Article

An Integrated High Throughput Experimentation/Predictive QSAR Modeling Approach to *ansa*-Zirconocene Catalysts for Isotactic Polypropylene

Christian Ehm ^{1,3,*} , Antonio Vittoria ^{1,3} , Georgy P. Goryunov ^{2,3} , Vyatcheslav V. Izmer ^{2,3},
Dmitry S. Kononovich ^{2,3}, Oleg V. Samsonov ^{2,3}, Rocco Di Girolamo ^{1,3} ,
Peter H. M. Budzelaar ^{1,3} , Alexander Z. Voskoboynikov ^{2,3}, Vincenzo Busico ^{1,3},
Dmitry V. Uborsky ^{2,3,*}  and Roberta Cipullo ^{1,3,*} 

¹ Dipartimento di Scienze Chimiche, Università di Napoli Federico II, Via Cintia, 80126 Napoli, Italy; antonio.vittoria@unina.it (A.V.); rocco.digirolamo@unina.it (R.D.G.); p.budzelaar@unina.it (P.H.M.B.); busico@unina.it (V.B.)

² Department of Chemistry, Lomonosov Moscow State University, 1/3 Leninskie Gory, 119991 Moscow, Russia; goryunov@org.chem.msu.ru (G.P.G.); izmer_slava@mail.ru (V.V.I.); dkononovich@org.chem.msu.ru (D.S.K.); oleg.samsonov@mail.ru (O.V.S.); voskoboy@med.chem.msu.ru (A.Z.V.)

³ Dutch Polymer Institute (DPI), P.O. Box 902, 5600 AX Eindhoven, The Netherlands

* Correspondence: christian.ehm@unina.it (C.E.); duborsky@med.chem.msu.ru (D.V.U.); rcipullo@unina.it (R.C.)

Received: 28 March 2020; Accepted: 18 April 2020; Published: 27 April 2020



Abstract: Compared to heterogeneous Ziegler–Natta systems (ZNS), *ansa*-metallocene catalysts for the industrial production of isotactic polypropylene feature a higher cost-to-performance balance. In particular, the C_2 -symmetric *bis*(indenyl) *ansa*-zirconocenes disclosed in the 1990s are complex to prepare, less stereo- and/or regioselective than ZNS, and lose performance at practical application temperatures. The golden era of these complexes, though, was before High Throughput Experimentation (HTE) could contribute significantly to their evolution. Herein, we illustrate a Quantitative Structure – Activity Relationship (QSAR) model trained on a robust and highly accurate HTE database. The clear-box QSAR model utilizes, in particular, a limited number of chemically intuitive 3D geometric descriptors that screen various regions of space in and around the catalytic pocket in a modular way thus enabling to quantify individual substituent contributions. The main focus of the paper is on the methodology, which should be of rather broad applicability in molecular organometallic catalysis. Then again, it is worth emphasizing that the specific application reported here led us to identify in a comparatively short time novel zirconocene catalysts rivaling or even outperforming all previous homologues which strongly indicates that the metallocene story is not over yet.

Keywords: olefin polymerization; stereoselectivity; regioselectivity; molecular weight capability; molecular catalysts; QSAR; i-PP

1. Introduction

Innovation in catalysis, i.e., the development of novel processes or products, selectivity or productivity enhancements for existing processes, etc., is a key driver of the chemical industry, and is typically a trial-and-error process. In recent times, the integration of High Throughput Experimentation (HTE) [1–8] with statistical modeling has been found to be a powerful accelerator. Regarding the latter, Quantitative Structure–Activity Relationship (QSAR) methods, originally

introduced in pharmaceutical chemistry [9], are now spreading in several domains of chemical R&D [10–13].

The polyolefin industry pioneered this trend. In the late 1990s, companies (e.g., Dow Chemical) engaged in massive HTE-based catalyst discovery programs [2,14–17], using parallel reactor setups and workflows pioneered by Symyx [4,18]. Those early applications focused on speed, that was often traded for accuracy at least in the so-called ‘primary screening’ stage. As a matter of fact, the initial identification of catalyst hits/leads was followed by structure optimization with conventional methods. More recently, in our labs we found ways to improve the precision and accuracy of the approach, by implementing highly controlled polymerization protocols on a state-of-the-art HTE reaction platform (Freeslate—former Symyx—Parallel Polymerization Reactor (PPR)), and integrating said platform with fast and thorough polymer characterization techniques, including Rapid-GPC, high-temperature cryoprobe ^{13}C NMR, Differential Scanning Calorimetry (DSC), and analytical Crystallization Elution Fractionation (aCEF) [19–24]. This workflow is now exploited to rapidly generate large catalyst structure-properties databases for optimization using predictive QSAR modeling [13]. In this paper, we illustrate how the approach was successfully applied to C_2 -symmetric *ansa*-zirconocene catalysts for the isotactic-selective polymerization of propene.

Known since the 1950s [25,26], Group 4 metallocenes gained credit as practical ethene polymerization catalysts in the mid-1970s, when the serendipitous discovery of the methylalumoxane (MAO) activator boosted productivity by several orders of magnitude [27,28]. In the following years, the simple unbridged bis(cyclopentadienyl) ligand framework was elaborated into a number of stereorigid bridged variants with different symmetries, including several precatalyst families with chirotopic active sites [29,30]. This opened the era of molecular stereoselective propene polymerization catalysis. A fierce R&D competition involved practically all polyolefin companies active at that time, and several billion USD were spent globally to identify molecular catalysts able to compete with classical heterogeneous Ziegler–Natta systems (ZNS) [22,31–35]. The main goal was the industrial production of isotactic polypropylene (i-PP), and by the end of the 1990s a number of companies had approached that target.

However, even the best champions in the field, such as the class of *rac*- $\text{Me}_2\text{Si}(2\text{-R}^1\text{-4-R}^2\text{-1-Indenyl})_2\text{ZrX}_2$ [36,37] complexes introduced by Spaleck and co-workers at Hoechst (Spaleck type zirconocenes), their homologues with fused aromatic cycles [38], and the ultra-rigid Hf-based homologues disclosed more recently by Rieger and co-workers [39,40], could not match the exceptional cost-to-performance balance of ZNS, particularly at industrially relevant temperatures ($\geq 70^\circ\text{C}$).

As a matter of fact, the market of metallocene i-PP has never grown above the size of a specialty niche (currently, less than 5% by volume of total i-PP production [31,32,41]). By the end of the last millennium, the perception that an upper limit had been attained became tangible in the chemical community [42], and from that time onward the research efforts declined rapidly. Notably, this was before HTE and QSAR modeling could contribute to any significant extent.

It may be worthy to recall at this point that, according to the definition in pharma, the QSAR is a mathematical function of the form [43]:

$$P_i = k'(D_{1i}, D_{2i}, \dots, D_{ni}) \quad (1)$$

where P_i are biological activities of a set of compounds of interest, D_{ji} are calculated (or, sometimes, experimentally measured) structural properties of said compounds (so-called ‘molecular descriptors’), and k' is some empirically established mathematical transformation (e.g., a linear or non-linear combination) that can be applied to descriptors to calculate P_i for all compounds in the examined set. The underlying principle is that compounds with similar structures are also characterized by similar activities, and the goal is to use k' in order to predict the activity of yet unknown compounds added to the set by interpolation or, possibly, by moderate extrapolation. An obvious (albeit sometimes overlooked) point is that no QSAR model can be of better quality than the experimental database on

which it was trained [43]: to guarantee solid and reliable predictions, a database must be large enough to avoid over-fitting, and accurate enough to yield a meaningful correlation.

When the concept is generalized in a broad chemical context, by ‘activity’ one must intend a number of different and often highly diversified performance properties. In the specific case of propene polymerization catalysts, these typically include monomer insertion rate, stereoselectivity, regioselectivity, and polymer molar mass capability. Among the several reasons why *ansa*-metallocenes, in general, represent excellent objectives for QSAR elaboration, an important one is that the stereorigid ligand framework greatly simplifies the design and quantification of well-working descriptors. That said, the fact that these catalysts can perform outstandingly has long been demonstrated [13,36,37,44–46]. The last decades have brought copious amounts of performance data in the literature, however, the extreme sensitivity of these catalysts to the activation protocol and use conditions renders the compilation of a coherent database for QSAR modeling from multiple literature sources nearly impossible [29,30,47–49].

Specifically, the *ansa*-bis(1-indenyl) frame is amenable to structural amplification with innumerable substitution patterns. However, the difficult and highly idiosyncratic multi-step protocols of ligand preparation, metalation, and isomeric purification of these compounds has long represented a major drawback for HTE. It was only recently that convenient methods of parallel synthesis and rapid purification were introduced [50,51].

Taking advantage of this progress, we assembled a library of 38 C_2 -symmetric *ansa*-zirconocene precatalysts with large structural diversity (Figure 1 and Supporting Information (SI)); of these, 22 were already known from the previous literature, whereas 16 are novel. Catalysts **M1–M19** feature exclusively variations in the 4-R position or in the bridge [13]. The newly added catalysts **M20–M38** expand the database to include variations in all other 1-indenyl positions (i.e., 2-, 3-, 5-, 6-, and 7-position), which have varying degrees of influence on polymerization performance.

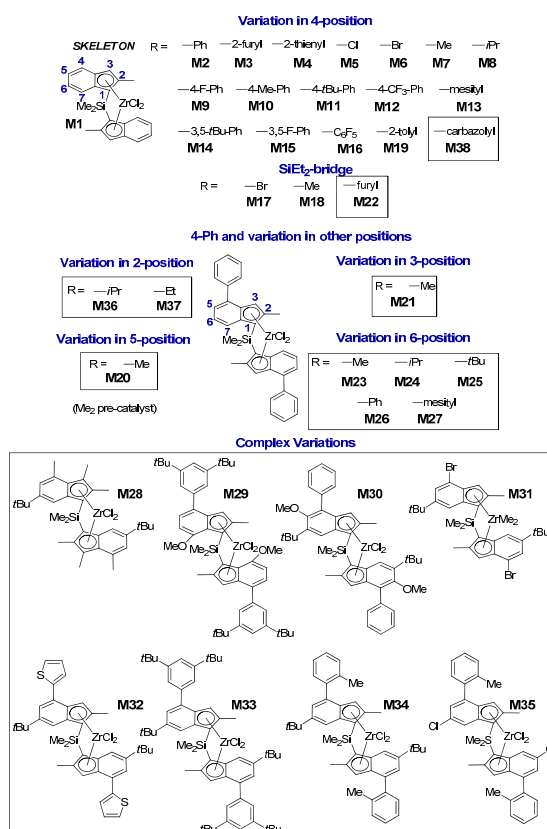


Figure 1. LZrCl₂ pre-catalysts **M1–M38** synthesized and screened in propene homopolymerization at $T_p = 60\text{ }^\circ\text{C}$ and $p(\text{C}_3\text{H}_6) = 6.6\text{ bar}$ in toluene. The performance of catalysts **M1–M19** which are part of the present Quantitative Structure – Activity Relationship (QSAR) study has been described in Reference [13].

All catalysts were screened in propene homopolymerization at $T_p = 60\text{ }^\circ\text{C}$ and $p(\text{C}_3\text{H}_6) = 6.6\text{ bar}$ in toluene solution using the aforementioned HTE workflow. These conditions were chosen to ensure that the side process of growing chain epimerization [29,30,52–55] was negligible [13,52,53]. The resulting database was used to train predictive QSAR models for stereoselectivity, regioselectivity and polymer molar mass capability. The predictive ability of the models was then tested on a validation set of five new catalysts (**M39–M43**) specifically prepared for the purpose.

2. Materials and Methods

Catalyst Synthesis: **M1** and **M2** were kindly donated by SABIC and used as received. **M6** and **M17** [56], **M4** [51], **M8** [36], **M7**, **M9**, **M10**, and **M13** [57] and **M11**, **M14**, and **M15** [58], **M26** [51], **M29** [39], **M30** [46], **M37** [59], **M38** [60], **M3**, **M5**, **M12**, **M16**, **M18**, and **M19** [13] were synthesized according to the literature. The synthesis of **M20–M28**, **M31–M36**, and **M39–M43** is detailed in the SI.

Polymer Synthesis and Characterization: All propene polymerization experiments were performed in toluene in a Freeslate Parallel Pressure Reactor (Freeslate, San Francisco, CA, USA) setup with 48 reaction cells (PPR48), fully contained in a triple MBraun glovebox under nitrogen. The cells, with a working volume of 5.0 mL, feature an 800 rpm magnetically coupled stirring, and individual online reading/control of temperature, pressure, monomer uptake, and uptake rate. The setup and the operating protocol, described in full detail in References [19,20], are reported in the SI and have been used successfully before in various homogeneous and heterogeneous polymerization studies [13,21,24]. Polymerization conditions were as follows (and identical to those used in Reference [13]): $T = 60\text{ }^\circ\text{C}$; $p(\text{C}_3\text{H}_6) = 4.5$ or 6.6 bar ; activator and scavenger $\text{Al}(\textit{iso}\text{-butyl})_3$ (TIBA)/*N,N*-dimethylanilinium tetrakis(perfluorophenyl)borate (AB) or MAO. Operating at two propene partial pressures was aimed

to verify that growing chain epimerization did not interfere under the investigated conditions. The catalysts were not pre-activated prior to injection into the PPR cells.

The polymers were characterized by: (a) high-temperature GPC with a Freeslate Rapid-GPC setup; (b) quantitative $^{13}\text{C}\{^1\text{H}\}$ NMR with a Bruker DRX 400 spectrometer equipped with a high-temperature cryoprobe (for 5 mm OD tubes) and a pre-heated robotic sample changer; and (c) DSC with a Mettler Toledo DSC-822 calorimeter (Columbus, OH, USA). Polymer melting points (T_m) were collected from the second heating scan. All results are averages on polymer samples produced in polymerization experiments performed in duplicate. More details can be found in the SI, Tables S1 and S2.

Computational Details: Geometries of LMCl_2 complexes were fully optimized using the Gaussian16 software package [61] in combination with the OPTIMIZE routine of Baker [62,63] and the BOpt software package [64]. Following the protocol proposed in Reference [65], all pre-catalysts were optimized at the TPSSTPSS/cc-pVDZ(-PP) [66–69] level of theory, using a small core pseudo potential on Zr [70,71]. The protocol has been successfully used, in combination with M06-2X [72] single-point energies (SP), to address several polymerization related problems: i.e., absolute barrier heights for propagation [73], comonomer reactivity ratios [74,75], metal-carbon bond strengths under polymerization conditions [76–78], electronic and steric tuning of M_w capability [79], and QSAR modeling [13]. The density fitting approximation (Resolution of Identity, RI) [80–83] and standard Gaussian16 quality settings [Scf = Tight and Int(Grid = Fine)] were used throughout. All structures represent true minima (as indicated by the absence of imaginary frequencies). Buried volume descriptors were calculated using the SambVca 2.0 program [84]. The Natural Population Analysis (NPA) charges were determined from SP calculations at the M06-2X/cc-pVTZ(-PP) level of theory using the NBO 3.0 program [85], implemented in Gaussian16. The minimum structure of **M3/M22** features the furyl rings oriented towards the center of the catalysts. In this case a structure with the furyl rings frozen in the angle found in the lowest insertion TS structure was used for the QSAR models, for more details see Reference [13].

QSAR Models: QSAR models consisting of up to five descriptors were built via multiple regression analysis (LINEST function). Accepted models show p -values < 0.05 for all contributing descriptors and the intercept. Leave-one-out analysis was performed with R in *RStudio*.

3. Results and Discussion

When the precatalysts of Figure 1 were activated in toluene solution with methylalumoxane (MAO) or a combination of $\text{Al}(\text{iso-butyl})_3$ and trityl tetrakis-perfluorophenylborate (TIBA/TTB), propene polymerization was in most cases too fast ($\text{TOF} > 10^3 \text{ s}^{-1}$ at $T = 60 \text{ }^\circ\text{C}$ and $p(\text{C}_3\text{H}_6) = 6.6 \text{ bar}$) for good reaction control in the small PPR reaction cells (5.0 mL working volume each). A protocol to modulate the reaction rate almost at will without affecting polymer properties was implemented using as the activator a combination of TIBA and N,N -dimethylanilinium tetrakis-perfluorophenylborate (AB) [86]. The PP samples for the present study were prepared purposely at moderate reaction rate (see Experimental Section and SI), and polymer properties (namely stereoregularity, regioregularity, and average molar mass) turned out to be highly reproducible (much more so than upon MAO or TIBA/TTB activation).

Notably, with several catalysts in the set the generation of stereodefects and/or chain termini turned out to fall under the definition of ‘rare events’ ($< 0.1\%$ of TOF). Measuring said microstructural features with high accuracy in HTE mode represented an extreme but also mandatory technical challenge [19–21], because *i*-PP properties depend crucially on them, and even minute differences in their fractional abundance have a strong impact on the polymer application window [87–90]. We managed to overcome the problem with the only exception of catalysts approaching ‘perfect’ stereoselectivity ($> 0.9998\%$), ranking such catalysts was not possible since the fraction of stereodefects in the polymers turned out to be lower than our ^{13}C NMR evaluation uncertainty ($\pm 0.02 \text{ mol}\%$).

The experimental QSAR database is summarized in Table 1. Catalyst stereoselectivity (enantioselectivity, σ , that is the mole fraction of monomer insertions with the preferred enantioface)

ranged between 0.9720 and >0.9998 (i.e., from 2.8 to <0.02 mol% stereoirregular monomeric units in the polymer); overall regioselectivity ($regio_{tot}$, that is the summed mole fractions of monomer insertions with 2,1 or 3,1 enchainments) between 0.9859 and 0.9991 (i.e., from 1.4 to 0.09 mol% regioirregular monomeric units); number-average polymer molar mass (M_n) between 10 and 1400 kDa. Two catalysts however produced poorly stereoregular oligomers for which neither stereo- nor regioselectivity could not be determined. The table also includes the melting temperature of the polymers measured by DSC. To the best of our knowledge, this database for the catalyst class of interest is unprecedented in terms of quality and robustness.

Table 1. Results of the characterization of polypropylene (PP) samples prepared at $T_p = 60$ °C and $p(C_3H_6) = 6.6$ bar in toluene with the 38 *ansa*-zirconocene catalysts of Figure 1 (see text for details).

| ID | Substituent Pattern | $Regio_{tot}$ [#] | $1-\sigma$ [‡] | M_n [*] | PDI ^{**} | T_m [‡] |
|------------------|--------------------------------|----------------------------|-------------------------|--------------------|-------------------|--------------------|
| M1 [†] | 2-Me | 0.29 | 1.35(3) | 100 | 1.9 | 145.7 |
| M2 [†] | 2-Me-4-Ph | 0.32 | 0.12 | 320 | 2.0 | 160.2 |
| M3 [†] | 2-Me-4-furyl | 0.91 | 0.80 | 130 | 2.1 | 143.2 |
| M4 [†] | 2-Me-4-thienyl | 0.50 | 0.29 | 230 | 2.0 | 153.2 |
| M5 [†] | 2-Me-4-Cl | 0.53 | 0.40 | 150 | 2.0 | 151.7 |
| M6 [†] | 2-Me-4-Br | 0.82 | 0.40 | 140 | 1.9 | 148.9 |
| M7 [†] | 2-Me-4-Me | 0.67 | 0.40 | 80 | 2.1 | 148.9 |
| M8 [†] | 2-Me-4- <i>i</i> Pr | 0.74 | 0.38 | 100 | 2.1 | 149.7 |
| M9 [†] | 2-Me-4-(4-F-Ph) | 0.29 | 0.11 | 320 | 2.1 | 157.3 |
| M10 [†] | 2-Me-4-(4-Me-Ph) | 0.40 | 0.14 | 230 | 2.4 | 157.6 |
| M11 [†] | 2-Me-4-(4- <i>t</i> Bu-Ph) | 0.30 | 0.14 | 250 | 2.2 | 159.3 |
| M12 [†] | 2-Me-4-(4-CF ₃ -Ph) | 0.32 | 0.11 | 290 | 2.4 | 156.9 |
| M13 [†] | 2-Me-4-mesityl | 0.40 | 0.03 | 80 | 2.2 | 155.3 |

Table 1. Cont.

| ID | Substituent Pattern | Regio _{tot} [#] | 1- σ [‡] | M _n [*] | PDI ^{**} | T _m [‡] |
|------------------|---|-----------------------------------|--------------------------|-----------------------------|-------------------|-----------------------------|
| M14 [†] | 2-Me-4-(3,5- <i>t</i> Bu-Ph) | 0.17 | 0.06 | 530 | 2.2 | 162.4 |
| M15 [†] | 2-Me-4-(3,5-F-Ph) | 0.42 | 0.16 | 290 | 2.3 | 157.2 |
| M16 [†] | 2-Me-4-C ₆ F ₅ | 0.18 | 0.06 | 410 | 2.2 | 160.8 |
| M17 [†] | 2-Me-4-Br, SiEt ₂ -bridge | 0.79 | 0.37 | 140 | 2.2 | 149.0 |
| M18 [†] | 2-Me-4-Me, SiEt ₂ -bridge | 0.66 | 0.41 | 90 | 2.3 | 149.3 |
| M19 [†] | 2-Me-4- <i>o</i> -tolyl | 0.42 | <0.02 | 470 | 1.8 | 158.2 |
| M20 | 2,5-Me-4-Ph | 0.48 | <0.02 | 610 | 2.1 | 158.2 |
| M21 | 2,3-Me-4-Ph | N/A | N/A | 1.0 | 2.2 | N/A |
| M22 | 2-Me-2-furyl, SiEt ₂ -bridge | 0.90 | 0.83 | 130 | 1.3 | 143.2 |
| M23 | 2,6-Me-4-Ph | 0.28 | 0.09 | 380 | 2.2 | 159.7 |
| M24 | 2-Me-4-Ph-6- <i>i</i> Pr | 0.54 | 0.10 | 630 | 2.3 | 156.1 |
| M25 | 2-Me-4-Ph-6- <i>t</i> Bu | 0.69 | 0.11 | 710 | 2.4 | 153.4 |
| M26 | 2-Me-4,6-Ph | 0.43 | 0.09 | 480 | 2.0 | 158.2 |
| M27 | 2-Me-4-Ph-6-mesityl | 0.98 | 0.22 | 490 | 2.2 | 148.4 |
| M28 | 2,3-Me-6- <i>t</i> Bu | N/A | N/A | 3 | 1.8 | N/A |
| M29 | 2-Me-4-(3,5- <i>t</i> Bu-Ph)-7-OMe | 0.23 | 0.03 | 400 | 2.2 | 162.2 |
| M30 | 2-Me-4-Ph-5-OMe-6- <i>t</i> Bu | 0.71 | 0.02 | 1400 | 2.3 | 156.0 |
| M31 | 2-Me-4-Br-6- <i>t</i> Bu | 1.41 | 0.33 | 290 | 2.0 | 143.0 |
| M32 | 2-Me-4-thienyl-6- <i>t</i> Bu | 1.05 | 0.31 | 620 | 2.3 | 148.0 |
| M33 | 2-Me-4-(3,5- <i>t</i> Bu-Ph)-6- <i>t</i> Bu | 0.30(3) | 0.05 | 950 | 2.3 | 160.6 |
| M34 | 2-Me-4- <i>o</i> -tolyl-6- <i>t</i> Bu | 0.83 | <0.02 | 990 | 2.3 | 154.3 |
| M35 | 2-Me-4- <i>o</i> -tolyl-6-Cl | 0.36 | 0.03 | 510 | 2.3 | 159.7 |
| M36 | 2- <i>i</i> Pr-4-Ph | 0.09 | 2.80(3) | 19 | 2.3 | 137.2 |
| M37 | 2-Et-4-Ph | 0.21 | 0.11 | 220 | 2.1 | 160.5 |
| M38 | 2-Me-4-(N-carbazolyl) | 0.20 | 0.04 | 800 | 2.3 | 161.5 |

Experimental conditions: T_p = 60 °C, toluene solvent, p(C₃H₆) = 6.6 bar, TIBA/AB activation (for abbreviations see text). Experimental uncertainty is ±2 on last significant digit for 1- σ and regio_{tot}, unless otherwise indicated in parentheses; ±20% on M_n. For more details see Supplementary Information (SI), Tables S1 and S2. [†] Data taken from Reference [13] [#] Total fraction of 2,1 and 3,1 monomeric units in % (¹³C NMR). [‡] Fraction of stereoirregular monomeric units in % (¹³C NMR), according to the enantiomorphic-site statistical model [29]. * In kDa. ** PDI = Poly-Dispersity Index (M_w/M_n). [‡] In °C. N/A: not available (the catalyst produced oligomers under the used conditions).

3.1. Experimental Trends and Hints for Descriptors

In the following, we highlight some experimental structure-property trends and correlations thereof with structural features of the catalyst precursors, calculated by Density Functional Theory (DFT). This qualitative survey was used to identify chemically intuitive descriptors for a ‘clear-box’ QSAR model (as will be explained in a following Section). The ‘classical’ catalyst precursor **M2** is used as a reference for comparative purposes.

3.1.1. Stereoselectivity

As is well-known, this property depends primarily on sterics and electronic effects can only have an indirect, albeit potentially devastating, impact in case they trigger the side process of growing chain epimerization [29,30,52–55]. When the popular ‘quadrant representation’ is adopted [91], it has been observed that maximizing the separation of steric bulk between ‘open’ and ‘closed’ quadrants is beneficial for stereoselectivity. This must be kept in mind when planning ligand substitution patterns (and is indeed well-captured by QSAR models, as we shall see later on).

Historically, substituents at positions 2 and 4 of a *rac-ansa*-bis(1-Indenyl) ligand frame were demonstrated to be crucial on all properties of importance for catalyst performance [36–38]. From a survey of our database, we concluded that the steric demand of substituents at 2-position negatively affects stereoselectivity whenever the steric bulk points towards the active pocket (see e.g., **M36**, Figure 2). Substituting 2- and 3-positions together can be highly detrimental, examples are **M21** and **M28**, yielding poorly stereoregular propene oligomers.

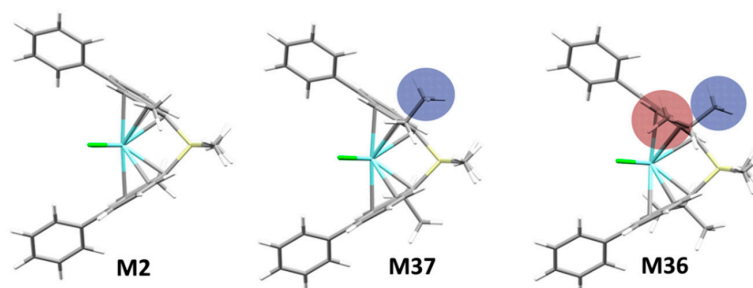


Figure 2. Increasing the steric demand of substituents at the 2-position negatively affects stereoselectivity if they intrude into the active pocket (see e.g., **M37** vs. **M36**). Stereoselectivity (σ): **M2** (2-Me) 0.9988 \approx **M37** (2-Et) 0.9989 > **M36** (2-*i*Pr) 0.9720.

The key role of 4-position substituents is well-known from the previous literature [36,37]. When the substituent is a phenyl (Ph), in particular, our data indicate that increasing the dihedral angle (β) between the phenyl and the indenyl plane (Figure 3) leads to an increase in σ , as separation of steric bulk between the ‘open’ and ‘closed’ quadrants is perfected [13]. Two alternative strategies to achieve this are either substituting the 4-Ph moiety itself (e.g., in **M19**, bearing a 4-*o*-Tolyl substituent), or the 5-position of the indenyl thus introducing a steric clash with the 4-Ph (e.g., in **M20** (5-Me) and **M30** (5-OMe)). We will refer to the former as a soft conformational lock, to the latter instead as a hard conformational lock. The lock function can be on the rigid indenyl catalyst backbone (hard lock, e.g., 5-Me) or on a flexible substituent on this rigid backbone (soft lock, e.g., *o*-Toluyyl).

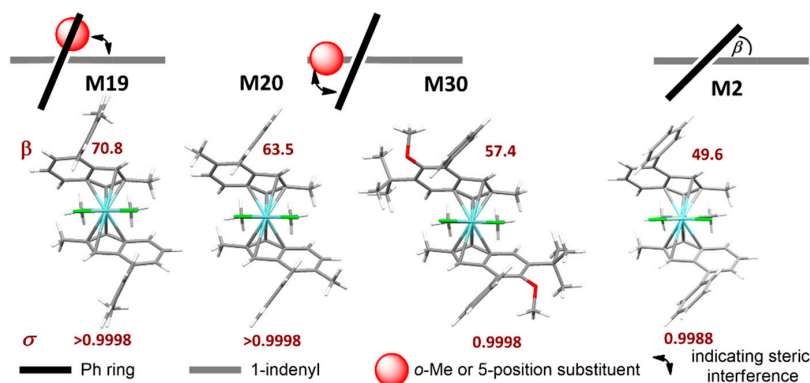


Figure 3. Effect of *ortho*-substituents of 4-Ph (4-*o*-Tolyl, **M19**), or substituents in the 5-position of the indenyl (**M20** and **M30**) on the dihedral angle (β) between the 4-Ph and the Indenyl plane, and consequent stereoselectivity σ . With increasing β the value of σ also increases, as separation of steric bulk between ‘open’ and ‘closed’ quadrants (see text) is perfected. **M2** data provided for comparison. Pictures generated with Mercury 4.2. Stylized sketches show upper indenyl ring (grey), phenyl substituent (black), and methyl or OMe substituent (red).

Both can lead to catalysts with near-to-perfect stereoselectivity (≤ 0.02 mol% stereoirregular insertions), e.g., **M19** (soft lock) and **M20** (hard lock); preliminary evidence suggests that the latter imparts superior rigidity to the molecule, which is beneficial for high-temperature application [92].

Substitution of 6-position is inconsequential for stereoselectivity, unless very bulky substituents are used, e.g., mesityl in **M27**. Finally, a 7-methoxy substituent (**M29**) increases stereoselectivity when compared to the same substituent pattern without it (**M14**). Rieger et al. have argued on the basis of crystal structure analysis that: (a) the stereoridity imparted by said methoxy substituent leads to lower values of ligand bite angle (α) [93] and Ph-Ind dihedral angle (β), and (b) this would be beneficial for the stereoselectivity (higher indeed for **M29** compared with **M2**) [94]. Gas phase DFT structures of a series of homologous precatalysts actually paint a different picture, and show that stereoselectivity primarily increases with increasing β (Table 2).

Table 2. Density Functional Theory (DFT)-calculated values of α and β angles (see text) vs. experimentally observed stereoselectivity σ for selected catalysts.

| Catalyst | α (°) * | β (°) | $1-\sigma$ † |
|------------|----------------|-------------|--------------|
| M2 | 60.5 | 49.6 | 0.12 |
| M14 | 60.5 | 51.1 | 0.06 |
| M29 | 60.2 | 52.8 | 0.03 |
| M30 | 60.9 | 56.1 | 0.02 |
| M20 | 60.9 | 63.5 | <0.02 |
| M19 | 60.8 | 70.8 | <0.02 |

* Bite angle or interplanar ring angle (α): angle formed by the two planes defined by the five carbon atoms of the C₅ fragments of the indenyl rings [93]. † Fraction of stereoirregular monomeric units in % (¹³C NMR), according to the enantiomeric-site statistical model [29].

3.1.2. Regioselectivity

Bulkier substituents in the 2-position like ethyl (**M37**) or *isopropyl* (**M36**) increase regioselectivity over that of **M2**, with **M36** showing the lowest amount of regioirregular monomeric units (0.09 mol%) in the entire polymer data set (Tables 1 and 3). This is in line with earlier conclusions that metallocene regioselectivity is mainly dictated by steric effects [95,96].

Table 3. 2-R substituent size vs. catalyst regioselectivity.

| Catalyst | 2-R Substituent | Regio _{tot} † |
|------------|-----------------|------------------------|
| M2 | Me | 0.32 |
| M37 | Et | 0.21 |
| M36 | iPr | 0.09 |

† Fraction of stereoirregular monomeric units in % (¹³C NMR), according to the enantiomeric-site statistical model [29].

We have shown earlier for catalysts **M1–M19** that perfecting the separation of steric bulk via tuning of the 4-position substituent enhances stereoselectivity and at the same time also benefits regioselectivity [13]. This is further confirmed by **M38** (4-(N-carbazoly)) [60], showing high stereoselectivity and fairly high regioselectivity (0.20 mol% regioirregular monomeric units in the polymer).

Electron-donating substituents in the 5- or 6-positions are mostly detrimental to regioselectivity. As an example, 6-*tert*-butyl substitution more than doubles regioirregular monomeric units in the polymer produced. The effect, however, is small or even negligible for small substituents (see e.g., 5-OMe, by comparing **M30** and **M25**; or 6-Me, by comparing **M23** with **M2**). Electron-withdrawing 6-Cl substitution (**M35**) increases regioselectivity somewhat (0.36 mol% regioirregular units for **M35**, instead of 0.42 mol% for **M19**). The 6-position is fairly remote from the active pocket, and one might be tempted to rule out steric effects of its substitution on regioselectivity. However, the lack of a consistent trend for the various electron-donating substituents in the set (compare e.g., 6-Me to 6-*t*Bu having opposing effects) likely points to a subtle balance between steric and electronic effects even in this distant position. 7-OMe substitution slightly lowers regioselectivity (from 0.17 mol% regioirregular units in the polymer for **M14** to 0.23 mol% for **M29**).

3.1.3. Molar Mass Capability

For the whole catalyst class of Figure 1 it has long been known that 2-Me substitution strongly increases average PP molecular weight [38]. This has been traced to a destabilization of the space-demanding 6-center TS of β -H transfer to the monomer [30,38], which is the dominant chain transfer pathway at least at moderate temperatures. Taking **M2** as a reference (2-Me; $M_n = 320$ kDa), larger alkyl groups in 2-position are detrimental in this respect, from moderately (**M37**, 2-Et; M_n 220 kDa) to very substantially (**M36**, 2-*i*Pr; M_n 19 kDa). The 3-position-substituted catalysts, in turn, yield essentially oligomers (see also SI, Figure S39).

Similar to regioselectivity, molar mass capability also increases when the distribution of steric bulk in the active pocket is perfected by 4-R substituent modulation [13]. **M38** (4-N-carbazolyl) confirms this further ($M_n = 800$ kDa). Introducing 5-position substituents approximately doubles molar mass capability of catalysts with a given substitution pattern. As shown before for stereoselectivity, this can be traced back to locking the 4-Ph substituent in a favorable β value. Any substituent in the 6-position increases molar mass capability, and the larger the substituent the higher the increase (Table 4).

Table 4. Effect of the 6-position substituents on the charge on the $ZrCl_2$ fragment (see text) and PP M_n (in kDa). For all catalysts 4-R = Ph.

| Catalyst | Substituent | M_n | $e^-_{ZrCl_2, NPA}$ | M_n Increase Factor |
|------------|-------------|-------|---------------------|-----------------------|
| M2 | H | 320 | 0.412 | - |
| M23 | Me | 380 | 0.405 | 1.2 |
| M26 | Ph | 480 | 0.412 | 1.5 |
| M24 | iPr | 630 | 0.404 | 2.0 |
| M25 | tBu | 710 | 0.403 | 2.2 |
| M30 | tBu + 5-OMe | 1400 | 0.400 | 4.4 |

6-Iso-propyl and 6-*tert*-butyl show very similar effects, both orienting two methyl groups towards the active pocket. Nifant'ev has proposed that the 5-OMe and 6-*tert*-butyl substituents of **M30** lower the electrophilicity of the Zr center, thus increasing molar mass capability over that of **M2** [46]. However, looking at the data series in Table 4, it appears that—again—steric effects are dominant over electronic effects, as the charge on the $ZrCl_2$ -fragment in all examined pre-catalysts is similar (actually almost identical for **M23** (6-Me), **M24** (6-*i*Pr), and **M25** (6-*t*Bu)).

Table 5 shows that introducing a 6-*tert*-butyl substituent into a given ligand has a near constant effect on PP M_n (1.8–2.7 fold increase) regardless of the remaining substituents. This is an interesting example of additive substituent effects for the catalyst class of interest.

Table 5. Effect of a 6-*t*Bu substituent on PP M_n (in kDa).

| Catalyst Pair | M_n without 6- <i>t</i> Bu | M_n with 6- <i>t</i> Bu | Increase Factor |
|----------------|------------------------------|---------------------------|-----------------|
| M2/M25 | 320 (M2) | 710 (M25) | 2.2 |
| M4/M32 | 230 (M4) | 620 (M32) | 2.7 |
| M6/M31 | 140 (M6) | 290 (M31) | 2.1 |
| M14/M33 | 530 (M14) | 950 (M33) | 1.8 |
| M19/M34 | 470 (M19) | 990 (M34) | 2.1 |

3.2. QSAR Modeling

The next step then was the identification of a convenient set of descriptors in order to implement a well-working QSAR model. Whereas this step is nowadays routine in pharmaceutical chemistry [9], with several software packages and libraries of descriptors available commercially, examples in organometallic catalysis are still rare [97], likely because—as we noted above—‘activity’ in the latter context indicates a whole set of performance properties that descend from different electronic and steric factors [10–13,84,98] and, moreover, can be difficult to quantify. In the following we define as a ‘clear-box’ QSAR model one which makes use of chemically intuitive descriptors with an evident meaning for the investigated systems (at odds with a ‘black-box’ QSAR model in which the descriptors are chosen tentatively out of very large sets, and selected for the best-working combination based on complex statistical procedures [9]). Out of the few literature clear-box QSAR studies in molecular olefin polymerization catalysis, the majority focused on the prediction of (relative) productivity in ethene or propene homopolymerization [10,12,99]. This property is in fact the nearest equivalent to ‘activity’ for pharma. At the same time however, it may not represent the best choice (at least in the context of interest here), considering the known sensitivity of most catalyst classes to: (a) the

activation protocol (which determines the fraction of active metal) [100,101], (b) the invariable presence of adventitious (and ubiquitous) impurities, and (c) a variety of deactivation routes [102]. On the other hand, clear-box QSAR models focusing on microstructural polymer features, e.g., for propene homopolymers or ethene/1-alkene copolymers, can be counted with two hands, possibly due to the lack of adequate experimental data. Cavallo proposed a simple descriptor based on the volume that the ligand occupies around the active metal (so-called ‘buried volume’) in order to predict the stereoselectivity and polymer molar mass capability of prototypical propene polymerization catalysts belonging to different families [42,84,101,103]. In a recent study, we found that this descriptor is indeed effective for accurate and fine predictions of stereoselectivity for a limited set of Spaleck-type zirconocenes, provided that the radius of the sphere centered on the transition metal used in the calculations is properly optimized in order to account for all relevant substituent effects [13]. The possible relevance of remote substituents on catalyst molar mass capability was claimed by Cruz [11].

3.2.1. QSAR Descriptors

Moving from these studies, we implemented a pool of seven descriptors, all related intuitively to simple electronic or steric properties of neutral $LZrX_2$ precatalysts that are easy to quantify with DFT methods (Figure 4 and SI) using previously established protocols (see experimental section for details) [61–83]. The six steric descriptors screen different regions of space around the catalyst, that were selected based on well-established olefin insertion and chain transfer transition state structures (SI, Table S4). Descriptors provides the fraction of hindered volume in a quadrant of a sphere centered on a certain atom (descriptors D3–D6), the difference in the fraction of hindered volume between open and closed quadrants (descriptor D1), or the summed fractions of hindered volume of two quadrants (descriptor D2) (see Figure 4, Tables S4 and S5). Altogether, the descriptors screen the distribution of steric hindrance in the catalytic pocket, so that mathematical optimization can fine-tune the impact of each region. It should be noted here that Cavallo’s buried volume model [103] works best for prediction of stereoselectivity when the separation of steric bulk between the quadrants is analyzed, not when the overall buried volume in the sphere is considered. Our approach is an extension to this: different regions of space are analyzed using various spheres, which ultimately also allows to account for different influences from different regions. This would be impossible using a single sphere. The Natural Population Analysis (NPA [85]) charge on the $ZrCl_2$ fragment turned out to perform satisfactorily as an electronic descriptor (D7).

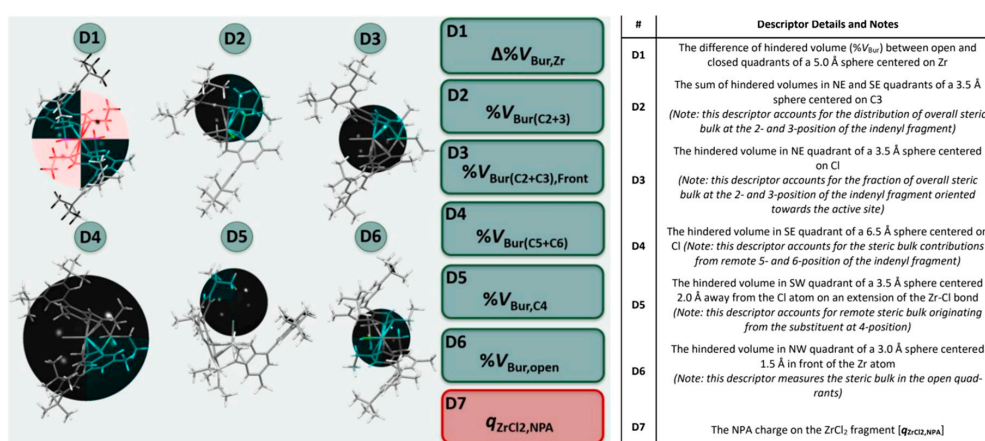


Figure 4. Computational descriptor pool for the *ansa*-zirconocenes of interest. 3D-steric descriptors D1–D6 were calculated using Cavallo’s SambVca 2.0 program. [84] Sphere position and size shown (black sphere), only quadrants with colored backbone are used for descriptor determination, all other quadrants are greyed out. D1–D4 and D6 shown so that the colored quadrant matches the description in the table. D5 has been rotated for clarity. (see SI, Tables S4 and S5 details on coordinate system definitions and construction of spheres and for further details).

3.2.2. QSAR Models

Linear combinations of said descriptors (Equation (1)) were tested in order to reproduce the performance properties of interest (quantified in terms of $\Delta\Delta G^\ddagger$ between the relevant competing events) for the 38 catalysts in the training set of Figure 1. The quantitative mathematical formulations of the best-fit models are given in the SI (Equations (S4)–(S6)), whereas the results are shown in Figure 5A–C and Table 6. An overview of which descriptors contribute to each model and in what sense is provided in Table 7.

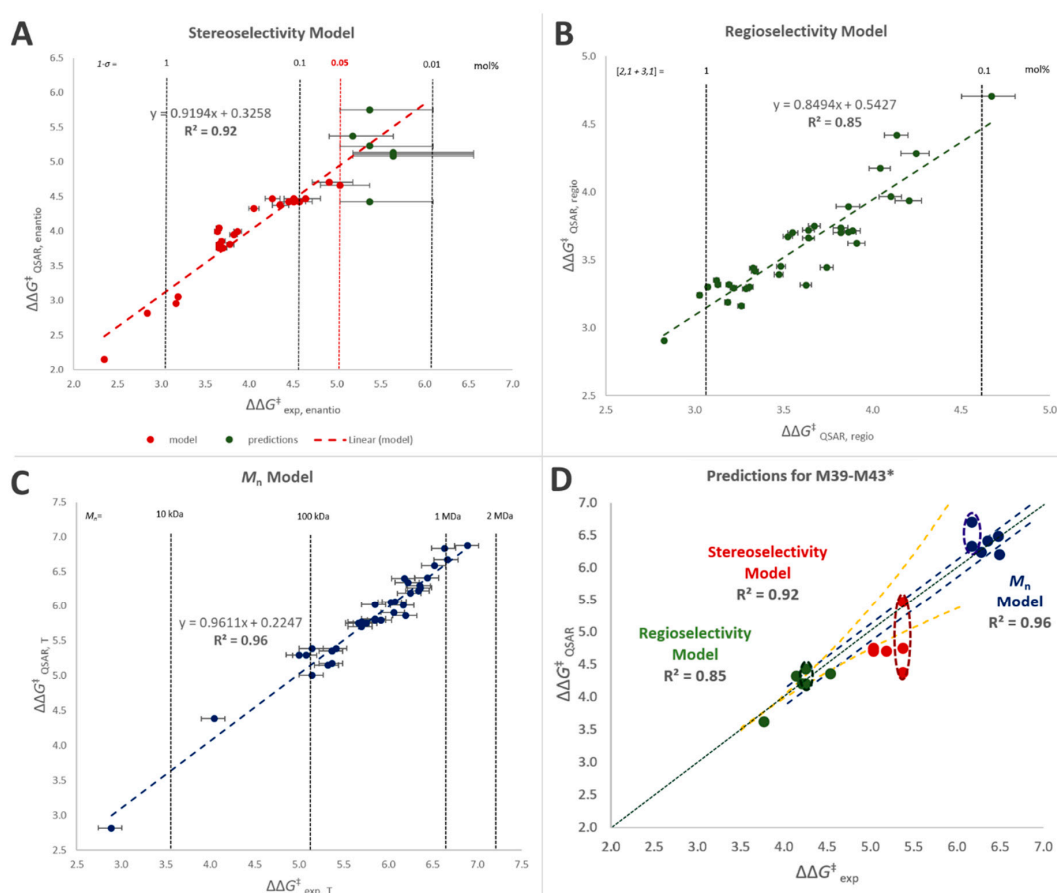


Figure 5. (A–C) QSAR-predicted vs. observed $\Delta\Delta G^\ddagger$ values (in kcal/mol) for the catalyst training set M1–M38 (Figure 1 and Table 1): stereoselectivity (A); regioselectivity (B); and polymer molar mass capability (C). The model for stereoselectivity was built using the available experimental data for $(1 - \sigma) \geq 0.05\%$ (see text). (D) QSAR-predicted vs. observed $\Delta\Delta G^\ddagger$ values for the catalyst validation set M39–M43 (Figure 6 and Table 8): stereoselectivity (red dots); regioselectivity (green dots); and polymer molar mass capability (blue dots). Green dotted line = perfect agreement. In all cases, error bars (yellow dotted lines: for stereo- and regioselectivity, blue dotted lines for molar mass capability) reflect experimental uncertainty (see Tables 1 and 8). * For M43 two conformational isomers of comparable stability were identified by DFT modeling (see SI); the calculated values of all polymer properties of interest are reported for each isomer, inscribed into dashed ellipses.

Stereoselectivity was satisfactorily reproduced as a function of descriptor D1 alone (Figure 5; $R^2 = 0.92$), which is not surprising in view of the previous literature, although the calculation protocol had to be customized (SI, Figures S41–S43). This notwithstanding, modeling the experimental data was complicated because, as already noted above, the error bar on $(1 - \sigma)$ explodes as soon as a catalyst approaches perfect stereoselectivity (Figure 5A). To solve this problem the model was trained on experimental values of $\sigma \leq 0.9995$, i.e., $(1 - \sigma) \geq 0.05\%$.

Regioselectivity and polymer molar mass capability, on the other hand, required linear combinations of five descriptors ($R^2 = 0.85$ and 0.96 , respectively). This was also to be expected, considering that, unlike stereoselectivity, both properties: (a) can be influenced via all seven substituent positions on the indenyl fragment, (b) may result from various molecular kinetic paths, and (c) can be influenced by steric and electronic effects.

The best-working model for regioselectivity does indeed make use of both electronic and steric descriptors, even though in agreement with previous computational studies the latter are dominating [98,104]. The best-working model for polymer molar mass capability, on the other hand, relies solely on steric descriptors. The outcome of key model assessment criteria, i.e., coefficient of determination (R^2), adjusted coefficient of determination (adj.- R^2) and cross validated R^2 via leave-one-out analysis (q^2), can be found in Table 6. Mean Average Deviation from Experiment (MAD) and Root Mean Square Error (RMSE) values are low (0.11–0.20 kcal/mol) for all models. Table 7 shows an overview of the impact of the different descriptors on each model.

Table 6. Key QSAR model assessment criteria.

| | $1-\sigma$ | $Regio_{tot}$ | M_n (kDa) |
|------------------------------------|--------------------|--------------------|--------------------|
| Data range (DR) | 2.8–0.05 | 1.41–0.09 | 3–1400 |
| DR in kcal/mol | 3.75 | 1.85 | 4.00 |
| R^2 /adj. R^2 | 0.92/0.92 | 0.85/0.82 | 0.96/0.95 |
| max. p -value | 4×10^{-8} | 2×10^{-3} | 1×10^{-4} |
| q^2 | 0.90 | 0.77 | 0.83 |
| MAD (kcal/mol) | 0.15 | 0.13 | 0.11 |
| MAD ($1-\sigma/regio_{tot}/M_n$) | 0.10 | 0.10 | 58 kDa |
| RMSE (kcal/mol) | 0.18 | 0.16 | 0.20 |

Table 7. List of used descriptors and their impact in the QSAR models for stereoselectivity, regioselectivity, and polymer molar mass capability.

| # | Regio | Stereo | M_n |
|----|-------|--------|-------|
| D1 | × | + | + |
| D2 | + | × | × |
| D3 | × | × | – |
| D4 | – | × | + |
| D5 | + | × | + |
| D6 | – | × | – |
| D7 | – | × | × |

+ = used in the linear combination with positive weight. – = used in the linear combination with negative weight.
 × = not used in the model.

3.2.3. Predictive QSAR Modeling

Once the training stage was satisfactorily finalized, we applied the QSAR models to anticipate the catalytic properties of novel catalysts. About 30 structures were screened in-silico, and classified with respect to the predicted performance and the ease of preparation (SI, Tables S19 and S20). Based on such criteria, five (pre)catalysts (M39–M43; Figure 6) were selected, prepared, and tested experimentally under the same conditions of M1–M38 (see SI for details). The results are summarized in Table 8.

All five turned out to perform remarkably well (see also Figure 7), and the agreement between experimental and QSAR-calculated properties is very nice (Figure 5D). M40 in particular turned out to outperform all catalysts in the training set.

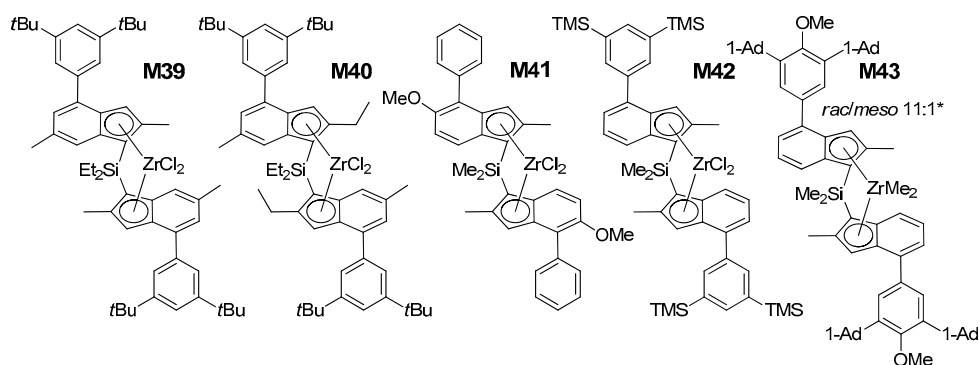


Figure 6. Structures of **M39–M43** (Ad = Adamantyl). * **M43** could not be further purified. The influence of varying the bridge from SiMe₂ to SiEt₂ is negligible within the experimental error margins [13].

Compared to Spaleck's archetype **M2**, it yielded i-PP samples with only 1/2 the amount of stereodefects (enantiodefects), 1/3 the amount of regioerrors, a 2-fold larger M_n value, and a two-fold higher productivity (with MAO activation, see SI, Table S3). Also with respect to the previous most balanced catalyst (**M14**) in Reference [13] a noticeable improvement in T_m is observed for **M40** (162.4 °C and 163.1 °C) and regioerrors are reduced by 1/3 to 0.11%. To the best of our knowledge, this T_m is the highest ever measured under the used polymerization conditions for this class of *ansa*-zirconocenes, and is indeed fairly close to that of ZNS i-PP.

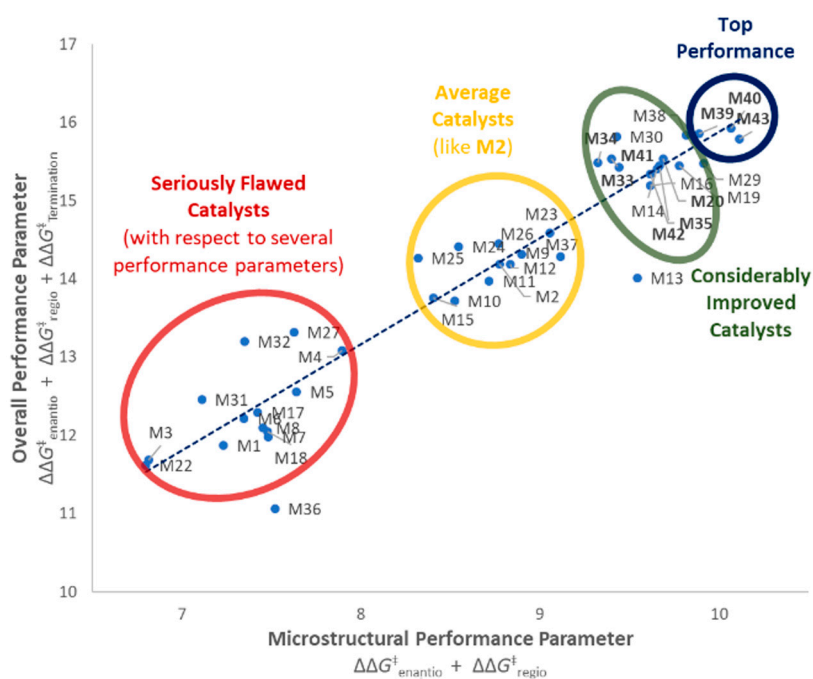


Figure 7. Performance balance of catalysts **M1–M43**. Blue trendline showing average trend of microstructural performance (stereo- and regioselectivity) vs. overall performance (including molar mass capability). Catalysts on the left of this line show higher molar mass capabilities than would be expected by this trend, catalysts on the right show lower ones. Three distinct catalyst groupings can be observed (seriously flawed to considerably improved). Nine out of 15 catalysts with considerable performance improvement (in bold) have been first reported in this manuscript, including the most balanced ones **M39**, **M40**, and **M43** (top performers).

Table 8. Predicted/observed (in bold) performance properties for catalysts **M39–M43**.

| QSAR/Exp. | 1- σ (%) | <i>Regio</i> _{tot} (%) | <i>M</i> _n (kDa) | <i>T</i> _m (°C) |
|------------|------------------------------|---------------------------------|-----------------------------|----------------------------|
| M39 | 0.08/0.04 | 0.17/0.18 | 760/740 | -/162.2 |
| M40 | 0.08/0.05 | 0.14/0.11 | 680/620 | -/163.1 |
| M41 | 0.08/0.04 | 0.42/0.35 | 490/760 | -/159.7 |
| M42 | 0.08/0.05 | 0.14/0.20 | 520/550 | -/161.6 |
| M43 | 0.02–0.12 ^a /0.03 | 0.12–0.15 ^a /0.17 | 1060–490 ^a /470 | -/162.6 |

^a The two pairs of QSAR-predicted values refer to two different precatalyst conformers identified by DFT, featuring the 1-Ad groups either oriented towards the active pocket or away from it, due to steric repulsion between 4-OMe and 3,5-Ad.

4. Conclusions

In the mid-1980s, *C*₂-symmetric *ansa*-bis(1-Indenyl) zirconocene catalysts represented the first compelling demonstration that highly isotactic-selective propene polymerization can be achieved with molecular catalysts, and even though several other classes of Group 4 *ansa*-metallocenes and post-metallocenes can now be used for that purpose they still represent the catalyst class of highest interest for industrial use. On the other hand, a higher cost-to-performance balance compared with classical ZNS has hampered large-scale application until now, and little progress in that respect has been reported in the last two decades.

In this paper, we have shown that state-of-the-art HTE-aided QSAR modeling can trigger new advances in the field. A structure-properties database of unprecedented size and robustness was rapidly assembled, and used to train and validate a clear-box QSAR model with predictive ability. The model utilizes, in particular, a limited number of chemically intuitive 3D geometric descriptors screening various regions of space in and around the catalytic pocket in a modular way that easily enables weighing and balancing the individual descriptor contributions to the overall catalytic performance.

In our opinion, the proposed HTE/QSAR approach represents a valuable tool for catalyst optimization of rather general validity, of course with proper adaptations and the more so the more steric effects are dominating. In the meantime, application to the class of *ansa*-zirconocenes covered is continuing, and we will report major advances in the near future.

Supplementary Materials: The following are available online at <http://www.mdpi.com/2073-4360/12/5/1005/s1>. Details for the synthesis of **M20–M28**, **M31–M36**, and **M39–M43**, including Figures S1–S38 with ¹H-NMR (odd numbers) and ¹³C-NMR (even numbers). Additional references relevant for synthesis [58,105–116]. Detailed polymerization procedure and results (Table S1: Propene Polymerization Experiments, Table S2: Full Polymer Characterization, Table S3: Performance of selected catalysts when activated with MAO). Figure S39: Experimental Trends - Deleterious Effect of the 3-Position Substituents on Molar Mass Capability. QSAR model details (Table S4: Descriptor list and reasons for inclusion of the descriptor in the descriptor pool, Figure S40: Differences between propene 1,2 and 2,1 insertion TS for **M39**, Table S5: Procedures for Descriptor Determination). QSAR models (Equations (S1)–(S6), Table S6: Experimental data used for QSAR modeling, Figure S41: Rationale for increased scanning sphere size to determine %*V*_{Bur,Zr} on the example of **M2**, Figure S42: Rationale for deletion of atoms or groups in the 5-, 6-, and 7-position and the Si-bridge to determine %*V*_{Bur,Zr}, Figure S43: Exclusion of atoms of the 2-position substituents not in line-of-sight of the active center for calculation of %*V*_{Bur,Zr}). QSAR model details, analysis of variance for QSAR models, leave-one-out analysis for QSAR models (Tables S7–S18), QSAR screening and synthesis candidates (Table S19: Predicted performance for selected catalysts, including **M39–M43** and Table S20: Estimated synthetic complexity, including **M39–M43**). Full Gaussian citation. (PDF) LMCl₂ structures (XYZ)

Author Contributions: Conceptualization, V.B. and A.Z.V.; methodology, C.E., R.C., and D.V.U.; formal analysis, C.E.; investigation, C.E., A.V., R.C., R.D.G., G.P.G., V.V.I., D.S.K. and O.V.S.; resources, V.B. and A.Z.V.; writing—original draft preparation C.E. and D.V.U.; writing—review and editing, C.E., R.C., P.H.M.B., V.B., D.V.U., and A.Z.V.; visualization, C.E. and G.P.G.; supervision, R.C., P.H.M.B., V.B., and A.Z.V.; funding acquisition, V.B. and A.Z.V. All authors have read and agreed to the published version of the manuscript.

Funding: This research was funded by the Dutch Polymer Institute, grant number 800.

Acknowledgments: This research forms part of the research program of DPI, project 800.

Conflicts of Interest: The authors declare no conflict of interest.

References

1. Hagemeyer, A.; Strasser, P.; Volpe, A.F., Jr. (Eds.) *High-Throughput Screening in Heterogenous Catalysis*; Wiley-VCH: Weinheim, Germany, 2004. [[CrossRef](#)]
2. Arriola, D.J.; Carnahan, E.M.; Hustad, P.D.; Kuhlman, R.L.; Wenzel, T.T. Catalytic Production of Olefin Block Copolymers via Chain Shuttling Polymerization. *Science* **2006**, *312*, 714–719. [[CrossRef](#)] [[PubMed](#)]
3. Robbins, D.W.; Hartwig, J.F. A Simple, Multidimensional Approach to High-Throughput Discovery of Catalytic Reactions. *Science* **2011**, *333*, 1423–1427. [[CrossRef](#)] [[PubMed](#)]
4. Boussie, T.R.; Diamond, G.M.; Goh, C.; Hall, K.A.; LaPointe, A.M.; Leclerc, M.; Lund, C.; Murphy, V.; Shoemaker, J.A.W.; Tracht, U.; et al. A Fully Integrated High-Throughput Screening Methodology for the Discovery of New Polyolefin Catalysts: Discovery of a New Class of High Temperature Single-Site Group (IV) Copolymerization Catalysts. *J. Am. Chem. Soc.* **2003**, *125*, 4306–4317. [[CrossRef](#)] [[PubMed](#)]
5. Diamond, G.M.; Hall, K.A.; LaPointe, A.M.; Leclerc, M.K.; Longmire, J.; Shoemaker, J.A.W.; Sun, P. High-Throughput Discovery and Optimization of Hafnium Heteroaryl-amido Catalysts for the Isospecific Polymerization of Propylene. *ACS Catal.* **2011**, *1*, 887–900. [[CrossRef](#)]
6. Allen, C.L.; Leitch, D.C.; Anson, M.S.; Zajac, M.A. The power and accessibility of high-throughput methods for catalysis research. *Nat. Catal.* **2019**, *2*, 2–4. [[CrossRef](#)]
7. Krska, S.W.; DiRocco, D.A.; Dreher, S.D.; Shevlin, M. The Evolution of Chemical High-Throughput Experimentation to Address Challenging Problems in Pharmaceutical Synthesis. *Acc. Chem. Res.* **2017**, *50*, 2976–2985. [[CrossRef](#)]
8. Shevlin, M. Practical High-Throughput Experimentation for Chemists. *ACS Med. Chem. Lett.* **2017**, *8*, 601–607. [[CrossRef](#)]
9. Cherkasov, A.; Muratov, E.N.; Fourches, D.; Varnek, A.; Baskin, I.I.; Cronin, M.; Dearden, J.; Gramatica, P.; Martin, Y.C.; Todeschini, R.; et al. QSAR Modeling: Where Have You Been? Where Are You Going To? *J. Med. Chem.* **2014**, *57*, 4977–5010. [[CrossRef](#)]
10. Cruz, V.L.; Martinez, J.; Martinez-Salazar, J.; Ramos, J.; Reyes, M.L.; Toro-Labbe, A.; Gutierrez-Oliva, S. QSAR model for ethylene polymerisation catalysed by supported bis(imino)pyridine iron complexes. *Polymer* **2007**, *48*, 7672–7678. [[CrossRef](#)]
11. Cruz, V.L.; Martinez, S.; Ramos, J.; Martinez-Salazar, J. 3D-QSAR as a Tool for Understanding and Improving Single-Site Polymerization Catalysts. A Review. *Organometallics* **2014**, *33*, 2944–2959. [[CrossRef](#)]
12. Manz, T.A. Deactivation of Ti and Zr half-metallocene complexes activated with B(C₆F₅)₃: A case study in constructing DFT-based QSARs to predict unimolecular rate constants. *RSC Adv.* **2015**, *5*, 48246–48254. [[CrossRef](#)]
13. Ehm, C.; Vittoria, A.; Goryunov, G.P.; Kulyabin, P.S.; Budzelaar, P.H.M.; Voskoboinikov, A.Z.; Busico, V.; Uborsky, D.V.; Cipullo, R. Connection of Stereoselectivity, Regioselectivity, and Molecular Weight Capability in *rac*-R'₂Si(2-Me-4-R-indenyl)₂ZrCl₂ Type Catalysts. *Macromolecules* **2018**, *51*, 8073–8083. [[CrossRef](#)]
14. Boussie, T.R.; Diamond, G.M.; Goh, C.; Hall, K.A.; LaPointe, A.M.; Leclerc, M.K.; Murphy, V.; Shoemaker, J.A.W.; Turner, H.; Rosen, R.K.; et al. Nonconventional Catalysts for Isotactic Propene Polymerization in Solution Developed by Using High-Throughput-Screening Technologies. *Angew. Chem. Int. Ed.* **2006**, *45*, 3278–3283. [[CrossRef](#)]
15. Frazier, K.A.; Boone, H.; Vosejka, P.C.; Stevens, J.C. High Activity Olefin Polymerization Catalyst and Process. U.S. Patent 6,953,764, 11 October 2005.
16. Peil, K.P.; Neithamer, D.R.; Patrick, D.W.; Wilson, B.E.; Tucker, C.J. Applications of High Throughput Research at The Dow Chemical Company. *Macromol. Rapid Commun.* **2004**, *25*, 119–126. [[CrossRef](#)]
17. Henry, W.; Turner, H.W. Impact of High-Throughput Screening Technologies on Chemical Catalysis. In *High-Throughput Screening in Heterogenous Catalysis*; Hagemeyer, A., Strasser, P., Volpe, A.F., Jr., Eds.; Wiley-VCH: Weinheim, Germany, 2004.
18. Murphy, V.; Bei, X.; Boussie, T.R.; Brümmer, O.; Diamond, G.M.; Goh, C.; Hall, K.A.; Lapointe, A.M.; Leclerc, M.; Longmire, J.M.; et al. High-Throughput Approaches for the Discovery and Optimization of New Olefin Polymerization Catalysts. *Chem. Rec.* **2002**, *2*, 278–289. [[CrossRef](#)] [[PubMed](#)]
19. Busico, V.; Cipullo, R.; Mingione, A.; Rongo, L. Accelerating the Research Approach to Ziegler–Natta Catalysts. *Ind. Eng. Chem. Res.* **2016**, *55*, 2686–2695. [[CrossRef](#)]

20. Busico, V.; Pellecchia, R.; Cutillo, F.; Cipullo, R. High-Throughput Screening in Olefin-Polymerization Catalysis: From Serendipitous Discovery Towards Rational Understanding. *Macromol. Rapid Commun.* **2009**, *30*, 1697–1708. [[CrossRef](#)]
21. Vittoria, A.; Meppelder, A.; Friederichs, N.; Busico, V.; Cipullo, R. Demystifying Ziegler–Natta Catalysts: The Origin of Stereoselectivity. *ACS Catal.* **2017**, *7*, 4509–4518. [[CrossRef](#)]
22. Vittoria, A.; Mingione, A.; Abbate, R.A.; Cipullo, R.; Busico, V. High Throughput Experimentation Protocol for Quantitative Measurements of Regioselectivity in Ziegler–Natta Polypropylene Catalysis. *Ind. Eng. Chem. Res.* **2019**, *58*, 14729–14735. [[CrossRef](#)]
23. Vittoria, A.; Meppelder, A.; Friederichs, N.; Busico, V.; Cipullo, R. Ziegler–Natta Catalysts: Regioselectivity and “Hydrogen Response”. *ACS Catal.* **2020**, *10*, 644–651. [[CrossRef](#)]
24. Vittoria, A.; Busico, V.; Cannavacciuolo, F.D.; Cipullo, R. Molecular Kinetic Study of “Chain Shuttling” Olefin Copolymerization. *ACS Catal.* **2018**, *8*, 5051–5061. [[CrossRef](#)]
25. Natta, G.; Pino, P.; Mazzanti, G.; Giannini, U. A Crystallizable Organometallic Complex Containing Titanium and Aluminum. *J. Am. Chem. Soc.* **1957**, *79*, 2975–2976. [[CrossRef](#)]
26. Breslow, D.S.; Newburg, N.R. Bis-(Cyclopentadienyl)-Titanium Dichloride—Alkylaluminum Complexes As Catalysts for The Polymerization of Ethylene. *J. Am. Chem. Soc.* **1957**, *79*, 5072–5073. [[CrossRef](#)]
27. Sinn, H.; Kaminsky, W.; Vollmer, H.-J.; Woldt, R. “Living Polymers” on Polymerization with Extremely Productive Ziegler Catalysts. *Angew. Chem. Int. Ed. Engl.* **1980**, *19*, 390–392. [[CrossRef](#)]
28. Kaminsky, W. Discovery of Methylaluminoxane as Cocatalyst for Olefin Polymerization. *Macromolecules* **2012**, *45*, 3289–3297. [[CrossRef](#)]
29. Busico, V.; Cipullo, R. Microstructure of polypropylene. *Prog. Polym. Sci.* **2001**, *26*, 443–533. [[CrossRef](#)]
30. Resconi, L.; Cavallo, L.; Fait, A.; Piemontesi, F. Selectivity in Propene Polymerization with Metallocene Catalysts. *Chem. Rev.* **2000**, *100*, 1253–1346. [[CrossRef](#)]
31. Gahleitner, M.; Resconi, L.; Doshev, P. Heterogeneous Ziegler–Natta, metallocene, and post-metallocene catalysis: Successes and challenges in industrial application. *MRS Bull.* **2013**, *38*, 229–233. [[CrossRef](#)]
32. Ali, S. Polyolefin Catalyst Market Overview. *Catal. Rev.* **2014**, *27*, 7.
33. Shamiri, A.; Chakrabarti, M.; Jahan, S.; Hussain, M.; Kaminsky, W.; Aravind, P.; Yehye, W. The Influence of Ziegler–Natta and Metallocene Catalysts on Polyolefin Structure, Properties, and Processing Ability. *Materials* **2014**, *7*, 5069. [[CrossRef](#)]
34. Pasquini, N. (Ed.) *Polypropylene Handbook*, 2nd ed.; Hanser Publishers: Munich, Germany, 2005.
35. Cecchin, G.; Morini, G.; Piemontesi, F.; Seidel, A. *Kirk-Othmer Encyclopedia of Chemical Technology*; Wiley-Interscience: New York, NY, USA, 2007; Volume 26.
36. Spaleck, W.; Antberg, M.; Rohrmann, J.; Winter, A.; Bachmann, B.; Kiprof, P.; Behm, J.; Herrmann, W.A. High Molecular Weight Polypropylene through Specifically Designe Zirconocene Catalysts. *Angew. Chem. Int. Ed. Engl.* **1992**, *31*, 1347–1350. [[CrossRef](#)]
37. Spaleck, W.; Kueber, F.; Winter, A.; Rohrmann, J.; Bachmann, B.; Antberg, M.; Dolle, V.; Paulus, E.F. The Influence of Aromatic Substituents on the Polymerization Behavior of Bridged Zirconocene Catalysts. *Organometallics* **1994**, *13*, 954–963. [[CrossRef](#)]
38. Stehling, U.; Diebold, J.; Kirsten, R.; Roell, W.; Brintzinger, H.H.; Juengling, S.; Muelhaupt, R.; Langhauser, F. ansa-Zirconocene Polymerization Catalysts with Anelated Ring Ligands—Effects on Catalytic Activity and Polymer Chain Length. *Organometallics* **1994**, *13*, 964–970. [[CrossRef](#)]
39. Schöbel, A.; Herdtweck, E.; Parkinson, M.; Rieger, B. Ultra-Rigid Metallocenes for Highly Iso- and Regiospecific Polymerization of Propene: The Search for the Perfect Polypropylene Helix. *Chem.-Eur. J.* **2012**, *18*, 4174–4178. [[CrossRef](#)]
40. Tranchida, D.; Mileva, D.; Resconi, L.; Rieger, B.; Schöbel, A. Molecular and Thermal Characterization of a Nearly Perfect Isotactic Poly(propylene). *Macromol. Chem. Phys.* **2015**, *216*, 2171–2178. [[CrossRef](#)]
41. Malpass, D.B.; Band, E.I. (Eds.) *Introduction to Industrial Polypropylene Properties, Catalysts, Processes*; Scriverener Publishing LLC: Beverly, MA, USA, 2012; p. 154. [[CrossRef](#)]
42. Falivene, L.; Cavallo, L.; Talarico, G. Buried Volume Analysis for Propene Polymerization Catalysis Promoted by Group 4 Metals: A Tool for Molecular Mass Prediction. *ACS Catal.* **2015**, *5*, 6815–6822. [[CrossRef](#)]
43. Tropsha, A. Best Practices for QSAR Model Development, Validation, and Exploitation. *Mol. Inform.* **2010**, *29*, 476–488. [[CrossRef](#)]

44. Resconi, L.; Balboni, D.; Baruzzi, G.; Fiori, C.; Guidotti, S.; Mercandelli, P.; Sironi, A. *rac*-[Methylene(3-tert-butyl-1-indenyl)₂]ZrCl₂: A Simple, High-Performance Zirconocene Catalyst for Isotactic Polypropene. *Organometallics* **2000**, *19*, 420–429. [[CrossRef](#)]
45. Reichelt, K.; Parkinson, M.; Resconi, L. Influence of Temperature on the Regioselectivity of Highly Isospecific C₂-Symmetric Zirconocenes in Propene Polymerization. *Macromol. Chem. Phys.* **2016**, *217*, 2415–2430. [[CrossRef](#)]
46. Nifant'ev, I.E.; Ivchenko, P.V.; Bagrov, V.V.; Churakov, A.V.; Mercandelli, P. 5-Methoxy-Substituted Zirconium Bis-indenyl *ansa*-Complexes: Synthesis, Structure, and Catalytic Activity in the Polymerization and Copolymerization of Alkenes. *Organometallics* **2012**, *31*, 4962–4970. [[CrossRef](#)]
47. Ehm, C.; Zaccaria, F.; Cipullo, R. From Mechanistic Investigation to Quantitative Prediction: Kinetics of Homogeneous Transition Metal-Catalyzed α -Olefin Polymerization Predicted by Computational Chemistry. In *Computational Quantum Chemistry—Insights into Polymerization Reactions*; Elsevier Inc.: Cambridge, MA, USA, 2019.
48. Severn, J.R.; Chadwick, J.C.; Duchateau, R.; Friederichs, N. “Bound but Not Gagged” Immobilizing Single-Site α -Olefin Polymerization Catalysts. *Chem. Rev.* **2005**, *105*, 4073–4147. [[CrossRef](#)] [[PubMed](#)]
49. Soga, K.; Ohgizawa, M.; Shiono, T.; Lee, D.H. Possibility of mass-transfer resistance in ethylene polymerization with magnesium chloride-supported catalysts. *Macromolecules* **1991**, *24*, 1699–1700. [[CrossRef](#)]
50. Ryabov, A.N.; Izmer, V.V.; Tzarev, A.A.; Uborsky, D.V.; Asachenko, A.F.; Nikulin, M.V.; Canich, J.A.M.; Voskoboynikov, A.Z. Palladium-Catalyzed Cross-Coupling Reactions of Bromo-Substituted Group 4 Metallocenes. *Organometallics* **2009**, *28*, 3614–3617. [[CrossRef](#)]
51. Izmer, V.V.; Lebedev, A.Y.; Nikulin, M.V.; Ryabov, A.N.; Asachenko, A.F.; Lygin, A.V.; Sorokin, D.A.; Voskoboynikov, A.Z. Palladium-Catalyzed Pathways to Aryl-Substituted Indenes: Efficient Synthesis of Ligands and the Respective *ansa*-Zirconocenes. *Organometallics* **2006**, *25*, 1217–1229. [[CrossRef](#)]
52. Busico, V.; Cipullo, R. Influence of Monomer Concentration on the Stereospecificity of 1-Alkene Polymerization Promoted by C₂-symmetric *ansa*-Metallocene Catalysts. *J. Am. Chem. Soc.* **1994**, *116*, 9329–9330. [[CrossRef](#)]
53. Busico, V.; Cipullo, R. Growing chain isomerizations in metallocene-catalyzed Ziegler–Natta 1-alkene polymerization. *J. Organomet. Chem.* **1995**, *497*, 113–118. [[CrossRef](#)]
54. Busico, V.; Caporaso, L.; Cipullo, R.; Landriani, L.; Angelini, G.; Margonelli, A.; Segre, A.L. Propene Polymerization Promoted by C₂-Symmetric Metallocene Catalysts: From Atactic to Isotactic Polypropene in Consequence of an Isotope Effect. *J. Am. Chem. Soc.* **1996**, *118*, 2105–2106. [[CrossRef](#)]
55. Busico, V.; Brita, D.; Caporaso, L.; Cipullo, R.; Vacatello, M. Interfering Effects of Growing Chain Epimerization on Metallocene-Catalyzed Isotactic Propene Polymerization. *Macromolecules* **1997**, *30*, 3971–3977. [[CrossRef](#)]
56. Voskoboynikov, A.Z.; Ryabov, A.N.; Nikulin, M.V.; Lygin, A.V.; Izmer, V.V.; Asachenko, A.F.; Coker, C.L.; Canich, J.A.M. Halogen Substituted Metallocene Compounds for Olefin Polymerization. U.S. Patent 7,446,216, 4 November 2008.
57. Voskoboynikov, A.Z.; Ryabov, A.N.; Coker, C.L.; Canich, J.A.M. Process for Producing Substituted Metallocene Compounds for Olefin Polymerization. U.S. Patent 7,709,670, 4 May 2010.
58. Voskoboynikov, A.Z.; Nikulin, M.V.; Ryabov, A.N.; Lygin, A.V.; Coker, C.L.; Canich, J.A.M. Preparation of Substituted Bridged Indenyl and Related Ligands. U.S. Patent 7,910,783, 22 March 2011.
59. Fujita, T.; Fukuoka, O.; Imuda, J.; Kawai, K.; Kiso, Y.; Nitahara, M.; Saito, J.; Tashiro, K.; Ueda, T.; Yoshida, M. New Transition Metal Compound, olefin Polymerization Catalyst Component Comprising the Same, Olefin Polymerization Catalyst containing this Component and Polymerization of Olefin. Japanese Patent JPH07286005A, 31 October 1995.
60. Izmer, V.V.; Lebedev, A.Y.; Kononovich, D.S.; Borisov, I.S.; Kulyabin, P.S.; Goryunov, G.P.; Uborsky, D.V.; Canich, J.A.M.; Voskoboynikov, A.Z. *ansa*-Metallocenes Bearing 4-(N-Azoly)l-2-methylindenyl and Related Ligands: Development of Highly Isoselective Catalysts for Propene Polymerization at Higher Temperatures. *Organometallics* **2019**, *38*, 4645–4657. [[CrossRef](#)]
61. Frisch, M.J.; Trucks, G.W.; Schlegel, H.B.; Scuseria, G.E.; Robb, M.A.; Cheeseman, J.R.; Scalmani, G.; Barone, V.; Petersson, G.A.; Nakatsuji, H.; et al. (Eds.) *Gaussian 16 Revision A.1*; Gaussian, Inc.: Wallingford, CT, USA, 2016; For full citation see SI.
62. Baker, J. An Algorithm for the Location of Transition-States. *J. Comput. Chem.* **1986**, *7*, 385–395. [[CrossRef](#)]
63. Baker, J. *PQS, 2.4*; Parallel Quantum Solutions: Fayetteville, AR, USA, 2001.

64. Budzelaar, P.H.M. Geometry optimization using generalized, chemically meaningful constraints. *J. Comput. Chem.* **2007**, *28*, 2226–2236. [[CrossRef](#)] [[PubMed](#)]
65. Ehm, C.; Budzelaar, P.H.M.; Busico, V. Calculating accurate barriers for olefin insertion and related reactions. *J. Organomet. Chem.* **2015**, *775*, 39–49. [[CrossRef](#)]
66. Tao, J.M.; Perdew, J.P.; Staroverov, V.N.; Scuseria, G.E. Climbing the density functional ladder: Nonempirical meta-generalized gradient approximation designed for molecules and solids. *Phys. Rev. Lett.* **2003**, *91*, 146401. [[CrossRef](#)]
67. Balabanov, N.B.; Peterson, K.A. Systematically convergent basis sets for transition metals. I. All-electron correlation consistent basis sets for the 3d elements Sc–Zn. *J. Chem. Phys.* **2005**, *123*, 064107. [[CrossRef](#)]
68. Balabanov, N.B.; Peterson, K.A. Basis set limit electronic excitation energies, ionization potentials, and electron affinities for the 3d transition metal atoms: Coupled cluster and multireference methods. *J. Chem. Phys.* **2006**, *125*, 074110. [[CrossRef](#)] [[PubMed](#)]
69. Schuchardt, K.L.; Didier, B.T.; Elsethagen, T.; Sun, L.; Gurumoorthi, V.; Chase, J.; Li, J.; Windus, T.L. Basis Set Exchange: A Community Database for Computational Sciences. *J. Chem. Inf. Model.* **2007**, *47*, 1045–1052. [[CrossRef](#)] [[PubMed](#)]
70. Schwerdtfeger, P. The Pseudopotential Approximation in Electronic Structure Theory. *ChemPhysChem* **2011**, *12*, 3143–3155. [[CrossRef](#)]
71. Peterson, K.A.; Figgen, D.; Dolg, M.; Stoll, H. Energy-consistent relativistic pseudopotentials and correlation consistent basis sets for the 4d elements Y–Pd. *J. Chem. Phys.* **2007**, *126*, 124101. [[CrossRef](#)]
72. Zhao, Y.; Truhlar, D.G. The M06 suite of density functionals for main group thermochemistry, thermochemical kinetics, noncovalent interactions, excited states, and transition elements: Two new functionals and systematic testing of four M06-class functionals and 12 other functionals. *Theor. Chem. Acc.* **2008**, *120*, 215–241. [[CrossRef](#)]
73. Ehm, C.; Cipullo, R.; Budzelaar, P.H.M.; Busico, V. Role(s) of TMA in polymerization. *Dalton Trans.* **2016**, *45*, 6847–6855. [[CrossRef](#)]
74. Zaccaria, F.; Ehm, C.; Budzelaar, P.H.M.; Busico, V. Accurate Prediction of Copolymerization Statistics in Molecular Olefin Polymerization Catalysis: The Role of Entropic, Electronic, and Steric Effects in Catalyst Comonomer Affinity. *ACS Catal.* **2017**, *7*, 1512–1519. [[CrossRef](#)]
75. Zaccaria, F.; Cipullo, R.; Budzelaar Peter, H.M.; Busico, V.; Ehm, C. Backbone rearrangement during olefin capture as the rate limiting step in molecular olefin polymerization catalysis and its effect on comonomer affinity. *J. Polym. Sci. A* **2017**, *55*, 2807–2814. [[CrossRef](#)]
76. Ehm, C.; Cipullo, R.; Passaro, M.; Zaccaria, F.; Budzelaar, P.H.M.; Busico, V. Chain Transfer to Solvent in Propene Polymerization with Ti Cp-phosphinimide Catalysts: Evidence for Chain Termination via Ti–C Bond Homolysis. *ACS Catal.* **2016**, *6*, 7989–7993. [[CrossRef](#)]
77. Ehm, C.; Budzelaar, P.H.M.; Busico, V. Metal–carbon bond strengths under polymerization conditions: 2,1-insertion as a catalyst stress test. *J. Catal.* **2017**, *351*, 146–152. [[CrossRef](#)]
78. Zaccaria, F.; Ehm, C.; Budzelaar, P.H.M.; Busico, V.; Cipullo, R. Catalyst Mileage in Olefin Polymerization: The Peculiar Role of Toluene. *Organometallics* **2018**, *37*, 2872–2879. [[CrossRef](#)]
79. Ehm, C.; Budzelaar, P.H.M.; Busico, V. Tuning the Relative Energies of Propagation and Chain Termination Barriers in Polyolefin Catalysis through Electronic and Steric Effects. *Eur. J. Inorg. Chem.* **2017**, *2017*, 3343–3349. [[CrossRef](#)]
80. Whitten, J.L. Coulombic potential energy integrals and approximations. *J. Chem. Phys.* **1973**, *58*, 4496. [[CrossRef](#)]
81. Baerends, E.J.; Ellis, D.E.; Ros, P. Self-consistent molecular Hartree–Fock–Slater calculations I. The computational procedure. *Chem. Phys.* **1973**, *2*, 41–51. [[CrossRef](#)]
82. Feyereisen, M.; Fitzgerald, G.; Komornicki, A. Use of approximate integrals in ab initio theory. An application in MP2 energy calculations. *Chem. Phys. Lett.* **1993**, *208*, 359–363. [[CrossRef](#)]
83. Vahtras, O.; Almlöf, J.; Feyereisen, M.W. Integral approximations for LCAO-SCF calculations. *Chem. Phys. Lett.* **1993**, *213*, 514–518. [[CrossRef](#)]
84. Falivene, L.; Credendino, R.; Poater, A.; Petta, A.; Serra, L.; Oliva, R.; Scarano, V.; Cavallo, L. SambVca 2. A Web Tool for Analyzing Catalytic Pockets with Topographic Steric Maps. *Organometallics* **2016**, *35*, 2286–2293. [[CrossRef](#)]

85. Glendening, E.D.; Badenhop, J.K.; Reed, A.E.; Carpenter, J.E.; Bohmann, J.A.; Morales, C.M.; Weinhold, F. *NBO 5.0*; Theoretical Chemistry Institute, University of Wisconsin: Madison, WI, USA, 2001.
86. Ehm, C.; Mingione, A.; Vittoria, A.; Zaccaria, F.; Cipullo, R.; Busico, V. High Throughput Experimentation in Olefin Polymerization Catalysis: Facing the Challenges of Miniaturization. manuscript in preparation.
87. De Rosa, C.; Auriemma, F.; Spera, C.; Talarico, G.; Tarallo, O. Comparison between Polymorphic Behaviors of Ziegler–Natta and Metallocene-Made Isotactic Polypropylene: The Role of the Distribution of Defects in the Polymer Chains. *Macromolecules* **2004**, *37*, 1441–1454. [[CrossRef](#)]
88. De Rosa, C.; Auriemma, F.; Di Capua, A.; Resconi, L.; Guidotti, S.; Camurati, I.; Nifant'ev, I.E.; Laishevstev, I.P. Structure–Property Correlations in Polypropylene from Metallocene Catalysts: Stereodeficient, Regioregular Isotactic Polypropylene. *J. Am. Chem. Soc.* **2004**, *126*, 17040–17049. [[CrossRef](#)] [[PubMed](#)]
89. De Rosa, C.; Auriemma, F.; Resconi, L. Influence of Chain Microstructure on the Crystallization Kinetics of Metallocene-Made Isotactic Polypropylene. *Macromolecules* **2005**, *38*, 10080–10088. [[CrossRef](#)]
90. De Rosa, C.; Auriemma, F.; Paolillo, M.; Resconi, L.; Camurati, I. Crystallization Behavior and Mechanical Properties of Regiodeficient, Highly Stereoregular Isotactic Polypropylene: Effect of Regiodefects versus Stereodeficient and Influence of the Molecular Mass. *Macromolecules* **2005**, *38*, 9143–9154. [[CrossRef](#)]
91. Corradini, P.; Guerra, G.; Cavallo, L. Do New Century Catalysts Unravel the Mechanism of Stereocontrol of Old Ziegler–Natta Catalysts? *Acc. Chem. Res.* **2004**, *37*, 231–241. [[CrossRef](#)]
92. Ehm, C.; Vittoria, A.; Di Girolamo, R.; Budzelaar, P.M.H.; Busico, V.; Cipullo, R.; Goryunov, G.P.; Izmer, V.V.; Kononovich, D.S.; Samsonov, O.V.; et al. Unpublished work. 2020.
93. Möhring, P.C.; Coville, N.J. Group 4 metallocene polymerisation catalysts: Quantification of ring substituent steric effects. *Coord. Chem. Rev.* **2006**, *250*, 18–35. [[CrossRef](#)]
94. Machat, M.R.; Lanzinger, D.; Pöthig, A.; Rieger, B. Ultrarigid Indenyl-based Hafnocene Complexes for the Highly Isoselective Polymerization of Propene: Tunable Polymerization Performance Adopting Various Sterically Demanding 4-Aryl Substituents. *Organometallics* **2017**, *36*, 399–408. [[CrossRef](#)]
95. Toto, M.; Cavallo, L.; Corradini, P.; Moscardi, G.; Resconi, L.; Guerra, G. Influence of π -Ligand Substitutions on the Regiospecificity and Stereospecificity in Isospecific Zirconocenes for Propene Polymerization. A Molecular Mechanics Analysis. *Macromolecules* **1998**, *31*, 3431–3438. [[CrossRef](#)]
96. Correa, A.; Talarico, G.; Cavallo, L. Regiochemistry of propene insertion with group 4 polymerization catalysts from a theoretical perspective. *J. Organomet. Chem.* **2007**, *692*, 4519–4527. [[CrossRef](#)]
97. Foscatto, M.; Jensen, V.R. Automated in Silico Design of Homogeneous Catalysts. *ACS Catal.* **2020**, *10*. [[CrossRef](#)]
98. Falivene, L.; Cao, Z.; Petta, A.; Serra, L.; Poater, A.; Oliva, R.; Scarano, V.; Cavallo, L. Towards the online computer-aided design of catalytic pockets. *Nature Chem.* **2019**, *11*, 872–879. [[CrossRef](#)] [[PubMed](#)]
99. Sanija, B.; Achary, P.G.R. Optimal Descriptor Based QSPR Models for Catalytic Activity of Propylene Polymerization. *Int. J. Quant. Struct.-Prop. Rel.* **2018**, *3*, 36–48. [[CrossRef](#)]
100. Bochmann, M. The Chemistry of Catalyst Activation: The Case of Group 4 Polymerization Catalysts. *Organometallics* **2010**, *29*, 4711–4740. [[CrossRef](#)]
101. Chen, E.Y.X.; Marks, T.J. Cocatalysts for metal-catalyzed olefin polymerization: Activators, activation processes, and structure-activity relationships. *Chem. Rev.* **2000**, *100*, 1391–1434. [[CrossRef](#)]
102. Crabtree, R.H. Deactivation in Homogeneous Transition Metal Catalysis: Causes, Avoidance, and Cure. *Chem. Rev.* **2015**, *115*, 127–150. [[CrossRef](#)]
103. Poater, A.; Cavallo, L. Comparing families of olefin polymerization precatalysts using the percentage of buried volume. *Dalton Trans.* **2009**, 8885–8890. [[CrossRef](#)]
104. Talarico, G.; Busico, V.; Cavallo, L. Origin of the Regiochemistry of Propene Insertion at Octahedral Column 4 Polymerization Catalysts: Design or Serendipity? *J. Am. Chem. Soc.* **2003**, *125*, 7172–7173. [[CrossRef](#)]
105. Nikulin, M.V.; Tsarev, A.A.; Lygin, A.V.; Ryabov, A.N.; Beletskaya, I.P.; Voskoboinikov, A.Z. Palladiumcatalyzed arylation of bis(4-bromo-2-methylinden-1-yl)dimethylsilane and related compounds. *Russ. Chem. Bull.* **2008**, *57*, 2298–2306. [[CrossRef](#)]
106. Resconi, L.; Castro, P.; Virkkunen, V.; Izmer, V.V.; Kononovich, D.S.; Kulyabin, P.S.; Voskoboinikov, A.Z. Catalysts. WO 2014096164A1, 26 June 2014.
107. Resconi, L.; Virkkunen, V.; Nouredine, A.; Castro, P.; Izmer, V.; Kononovich, D.; Voskoboinikov, A. Catalyst. WO 2014096282A1, 26 June 2014.

108. Resconi, L.; Castro, P.; Virkkunen, V.; Izmer, V.V.; Kononovich, D.S.; Kulyabin, P.S.; Voskoboynikov, A.Z. Catalysts. WO2014096166A1, 26 June 2014.
109. Voskoboynikov, A.Z.; Asachenko, A.F.; Kononovich, D.S.; Nikulin, M.V.; Tsarev, A.A.; Maaranen, J.; Vanne, T.; Kauhanen, J.; Mansner, E.; Kokko, E.; et al. Catalysts. WO2009027075A1, 5 March 2009.
110. Voskoboynikov, A.Z.; Ryabov, A.N.; Nikulin, M.V.; Lygin, A.V.; Coker, C.L.; Canich, J.A.M. Halogen Substituted Metallocene Compounds for Olefin Polymerization. WO 2007070041A1, 21 June 2007.
111. Resconi, L.; Focante, F.; Balboni, D.; Nifant'ev, I.E.; Ivchenko, P.V.; Bagrov, V. Metallocene Compounds. WO2007116034A1, 18 October 2007.
112. Canich, J.A.M.; Jiang, P.; Casty, G.L.; Kiss, G.; Voskoboynikov, A.Z.U.S. Production of Propylene-Based Polymers. U.S. Patent 7812104B2, 12 October 2010.
113. Matsubara, K.; Ueno, K.; Shibata, Y. Synthesis and Structures of Nickel Halide Complexes Bearing Mono- and Bis-coordinated *N*-Heterocyclic Carbene Ligands, Catalyzing Grignard Cross-Coupling Reactions. *Organometallics* **2000**, *25*, 3422–3427. [[CrossRef](#)]
114. Zhang, X.; Zhu, Q.; Guzei, I.A.; Jordan, R.F. General Synthesis of Racemic Me₂Si-Bridged Bis(indenyl) Zirconocene Complexes. *J. Am. Chem. Soc.* **2000**, *122*, 8093–8094. [[CrossRef](#)]
115. Sevov, C.S.; Hartwig, J.F. Iridium-Catalyzed Oxidative Olefination of Furans with Unactivated Alkenes. *J. Am. Chem. Soc.* **2014**, *136*, 10625–10631. [[CrossRef](#)] [[PubMed](#)]
116. Sam, J.; Plampin, J.N. Hypotensive Basic Ethers in the Indan Series. *J. Am. Chem. Soc.* **1960**, *82*, 5205–5209. [[CrossRef](#)]



© 2020 by the authors. Licensee MDPI, Basel, Switzerland. This article is an open access article distributed under the terms and conditions of the Creative Commons Attribution (CC BY) license (<http://creativecommons.org/licenses/by/4.0/>).